*R*esearch in
*A*stronomy and
*A*strophysics

Multifrequency emission analysis of TeV blazars H 2356–309 and 1ES 1218+304 [*]

Yun-Yong Tang[1], Zu-Cheng Dai[2] and Li Zhang[1]

[1] Department of Physics, Yunnan University, Kunming 650091, China; *tangyunyong888@163.com*
[2] Department of Physical Science and Technology, Kunming University, Kunming 650031, China

Abstract The multiband nonthermal emissions in radio, X-ray, and very high-energy (VHE) γ-ray bands from two distant blazars, H 2356–309 and 1ES 1218+304, have been detected, and, especially from recent observations with the Suzaku, MAGIC and VERITAS telescopes, clearly reveal nonthermal power-law spectra. We study the broadband nonthermal spectra of the two sources by using a combination of a one-zone homogeneous synchrotron self-Compton (SSC) model and an inhomogeneous conical jet model, where the new external background light (EBL) model is taken into account. The results show that (1) the nonthermal emissions of the two blazars, ranging from X-rays to VHE γ-rays, are from the homogeneous zone whereas the emissions in the radio bands can be explained as the radiation from the inhomogeneous conical jet; (2) a strict lower-limit EBL model can be used to explain their observed spectra well.

Key words: radiation mechanisms — active-BL Lacertae objects — TeV blazars: individual (H 2356–309, 1ES 1218+304)

1 INTRODUCTION

According to their observations, Active Galactic Nuclei (AGNs) are divided into two classes: radio-loud AGNs and radio-quiet AGNs. Blazars (including BL Lacertae objects and flat-spectrum radio quasars (FSRQs)), which are characterized by a non-thermal continuum spectrum and variability on time scales of minutes up to years, belong to the most extreme objects in radio-loud AGNs. Their broadband spectra have two obvious continuum components. The first component peaks between the infrared (IR) and the hard X-ray bands. In view of the location of this peak, BL Lacertae objects are further divided into the high-frequency peaked BL Lacertae objects (HBLs, ultraviolet (UV) to X-rays) and the low-frequency peaked BL Lacertae objects (LBLs, IR to optical) (Giommi & Padovani 1994). The second component peaks at higher energies and can extend to the VHE γ-ray band.

The emission models for TeV blazars mainly include hadronic and leptonic models. In the hadronic models, the protons are assumed to be initially accumulated and produce $e^{\pm}$ pairs via p-p or p-γ interactions (e.g., Mannheim & Biermann 1992; Mannheim 1993; Mücke & Protheroe 2000; Mücke et al. 2003; Pohl & Schlickeiser 2000; Dermer 1999; Atoyan & Dermer 2003). These pairs produce high-energy photons via synchrotron emission and inverse Compton scattering, and then

---

some high energy photons escape directly from the source, and others produce new pairs through $\gamma\gamma \rightarrow e^{\pm}$ pair interactions. New high energy photons are again generated by these new pairs. Such a process is described as proton initiated cascades (Mannheim 1993). In addition, the direct synchrotron emission from extreme high energy protons is also considered to be a possibility (Aharonian 2000), and the synchrotron emission of secondary muons and mesons can also be taken into account to build a self-consistent synchrotron-proton blazar (SPB) model (Rachen & Mészáros 1998; Mücke et al. 2003). Therefore, the electromagnetic cascades (e.g., π^0 cascade, $\pi^{\pm}$ cascade, p-synchrotron cascade and $\mu^{\pm}$-synchrotron cascade) can generate γ-rays, and the geometry of this model can be found in Böttcher (2007), but there are still some difficulties in explaining the broadband spectrum with hadronic models (e.g., Böttcher 2007). Here we only consider the leptonic models.

In the leptonic models, the synchrotron emission of the relativistic electrons accelerated in the jet results in the radio to X-ray continuum emission, while the γ-ray emission is produced via the inverse-Compton (IC) mechanism. At present, the synchrotron self-Compton (SSC) process is the most popular version. In this version, it is considered that the scattered soft photons are generated by the same electrons as those in the synchrotron emission mechanism (e.g., Marscher & Gear 1985; Maraschi et al. 1992; Ghisellini & Madau 1996; Inoue & Takahara 1996; Kataoka et al. 1999; Chiaberge & Ghisellini 1999; Katarzyński et al. 2001; Krawczynski et al. 2002; Finke et al. 2008). Additionally, if the low-energy photons are from other regions, such as the accretion disk, the clouds or other components of the jet itself, this scenario is described by external inverse-Compton (EIC) models (e.g., Sikora et al. 1994; Dermer et al. 1997; Sambruna et al. 1997; Błażejowski et al. 2000; Hartman et al. 2001; Böttcher & Reimer 2004; Kusunose & Takahara 2005).

TeV blazars H 2356–309 and 1ES 1218+304 are the two distant blazars observed at TeV γ-rays. Since the X-ray emission of H 2356–309 was first observed by the UHURU Satellite (Forman et al. 1978), the multiband data have been obtained from the BeppoSAX, the Archival (Superina et al. 2006), and so on. In particular, the simultaneous observations from the NRT (Nancay decimetric radio telescope), ROTSE (Robotic Optical Transient Search Experiment), RXTE (Rossi X-ray Timing Explorer) and H.E.S.S. (High Energy Stereoscopic System) telescopes are very significant for modeling the nonthermal spectra of H 2356–309. For the 1ES 1218+304, the NED database and the BeppoSAX telescope have offered data from radio emissions up to X-rays. The X-ray observations from the 1ES 1218+304 have been performed with Suzaku, and the VHE γ-rays were also recently detected by MAGIC and VERITAS. Their X-ray spectra both show a clear cut-off shape. Therefore, it is worth modeling their spectral energy distributions (SEDs) with these useful data.

In this paper, we model the SEDs of H 2356–309 and 1ES 1218+304 using a combination of the one zone homogeneous SSC model and the inhomogeneous jet model, where the new external background light (EBL) model is included. In Section 2, we briefly introduce these emission models and the absorption by $\gamma + \gamma \rightarrow e^+ + e^-$ interactions with photons from the extragalactic background light. In Section 3, we apply the models to two TeV blazars H 2356–309 and 1ES 1218+304. Finally, a brief summary and discussion are given in Section 4.

2 EMISSION MODELS AND HIGH ENERGY PHOTON ABSORPTION

We now describe the basic physics used in this paper. Considering a "blob in jet" scenario, a homogeneous blob is located inside the jet at the position R_x (see the next sections for details), and the blob can be seen as a shock traveling down the jet. Any increase in the pressure of the conical jet flow will result in the formation of a shock. Generally, the shock components should have a Lorentz factor with a value much larger than the jet. Because of extremely energetic disturbances of the jet flow, the shock Lorentz factor could exceed that of the jet by a factor of 2 or more (e.g., Marscher & Gear 1985; Lind & Blandford 1985; O'dell 1988; Katarzyński et al. 2001). In this paper, to simplify, we assume that the blob and the jet move along the same straight line. Although the jet is inhomogeneous due to the variable magnetic field and the uneven electron energy distribution in this

model, the Doppler factor in the jet was considered as a constant. For the blob, we could also only estimate its Doppler factor by the observational data and some physical parameters in the theoretical model. The detailed model will be discussed in the following parts. At first, we briefly introduce the one zone SSC model in which a single homogeneous emitting region is considered (Katarzyński et al. 2001). Secondly, the inhomogeneous jet model given by Ghisellini et al. (1985) can fit the low-energy spectra. Finally, we consider high energy photon absorption in calculating very high energy spectra.

2.1 One Zone SSC Model

In the one zone SSC model, it is assumed that a spherical blob with radius R_b moves with a relativistic speed, and the bulk Lorentz factor of the outflow is $\Gamma = (1 - \beta^2)^{-1/2}$, where $\beta = v_b/c$, and v_b is the velocity of the blob. The blob with a uniform magnetic field B is filled with nonthermal relativistic electrons with a uniform density. The electron energy distribution in the comoving frame of the blob can be described by the following partial differential equation:

$$\frac{\partial N(\gamma, t)}{\partial t} + \frac{N(\gamma)}{t_{\mathrm{e,esc}}} = \frac{\partial}{\partial \gamma}\left[(C_{\mathrm{cool}}(\gamma, t) - C_{\mathrm{acc}}(\gamma, t))N(\gamma, t)\right] + Q(\gamma, t), \tag{1}$$

where $\gamma = E/mc^2$ is the electron Lorentz factor, $t_{\mathrm{e,esc}}$ is the electron escape time from the emission region, $Q(\gamma, t)$ is the distribution of fresh electrons into the blob, C_{cool} and C_{acc} are the synchrotron self-Compton cooling rate and the acceleration rate, respectively. The solution of Equation (1) has been studied in detail by some previous papers (e.g., Kardashev 1962; Kirk et al. 1998; Chiaberge & Ghisellini 1999). Here, we use a good approximation (Katarzyński et al. 2001) and describe the electron energy distribution as follows:

$$N(\gamma) = \begin{cases} K\gamma^{-n_1} & (\gamma_{\min} \leq \gamma \leq \gamma_{\mathrm{brk}}) \\ K\gamma_{\mathrm{brk}}^{n_2-n_1}\gamma^{-n_2} & (\gamma_{\mathrm{brk}} \leq \gamma \leq \gamma_{\mathrm{cut}}) \end{cases}, \tag{2}$$

where K is the density of the electrons with $\gamma = 1$. Before the high energy emission spectra can be reproduced, we must constrain many parameters, such as R_b, $\gamma_{\min}$, γ_{brk}, γ_{cut}, etc. The available observed quantities allow us to deduce some free parameters (e.g., Tavecchio et al. 1998; Katarzyński et al. 2001, 2003). For instance, we can get an estimate of the Doppler factor $\delta_b = [\Gamma(1 - \beta\cos\vartheta)]^{-1}$ in view of the peak frequencies and the corresponding fluxes in the synchrotron spectrum and the inverse-Compton spectrum; ϑ is the angle between the jet and the observer's line of sight. Finally, we can estimate $R_b \leq c\delta_b t/(1+z)$ using the relationship between the variability timescale t' in the blob frame and the observed variability timescale t: $t' = \delta_b t/(1+z)$.

For a uniform isotropic radiation field, the synchrotron emission coefficient in units of erg cm^{-3} s^{-1} Hz^{-1} sr^{-1} for the electron energy distribution $N(\gamma)$ can be described as (Crusius & Schlickeiser 1986; Ghisellini et al. 1988)

$$j_s'\left(\nu_s'\right) = c_2 B \int_{\gamma_{\min}}^{\gamma_{\mathrm{cut}}} d\gamma N(\gamma) F\left(\frac{\nu_s'}{c_1 B\gamma^2}\right), \tag{3}$$

where $c_1 = 3e/4\pi m_e c$, $c_2 = \sqrt{3}e^3/4\pi m_e c^2$, ν_s' is the frequency in the comoving frame of the blob, and $F(x) = x\int_x^\infty K_{5/3}(y)dy$, where $K_{5/3}(y)$ is a modified Bessel function of the second kind of order 5/3. On the other hand, the synchrotron self-absorption coefficient in units of cm^{-1} is given by (e.g., Rybicki & Lightman 1979):

$$k_s'(\nu_s') = -\frac{c_3 B}{\nu_s'^2} \int_{\gamma_{\min}}^{\gamma_{\mathrm{cut}}} d\gamma \gamma^2 \frac{d}{d\gamma}\left[\frac{N(\gamma)}{\gamma^2}\right] F(\frac{\nu_s'}{c_1 B\gamma^2}), \tag{4}$$

where $c_3 = \sqrt{3}e^3/8\pi m_e c^2$. Therefore, the synchrotron emission intensity in units of erg cm^{-2} s^{-1} Hz^{-1} sr^{-1} is written as (e.g., Bloom & Marscher 1996; Kataoka et al. 1999)

$$I_s'(\nu_s') = \frac{j_s'(\nu_s')}{k_s'(\nu_s')}(1 - \frac{2}{\tau^2}[1 - e^{-\tau}(\tau + 1)]), \tag{5}$$

where $\tau = 2R_b k_s'(\nu_s')$ is the optical depth of the blob along the line of sight. Because of the Doppler boosting effect, the observed flux density can be described by (Katarzyński et al. 2001)

$$F_s(\nu_s') = \pi\delta_b^3(1 + z)\frac{R_b^2}{d_L^2}I_s'(\nu_s'), \tag{6}$$

where $d_L = 2c[z + 1 - (z + 1)^{1/2}]/H_0$ is the luminosity distance, and H_0 is the Hubble constant.

The number density of the synchrotron photons per energy interval is shown as follows (Kataoka et al. 1999)

$$n_s(\epsilon_s') = \frac{3}{4}\frac{4\pi}{hc\epsilon_s'}\frac{j_s'(\nu_s')}{k_s'(\nu_s')}\left[1 - e^{(-k_s'(\nu_s')R_b)}\right]. \tag{7}$$

For isotropic photon and electron distributions, the SSC emission coefficient is given by (Jones 1968; Blumenthal & Gould 1970)

$$j_c'(\nu_c') = \frac{h\epsilon_c'}{4\pi}\int d\epsilon_c' n_s(\epsilon_s')\int d\gamma N(\gamma)F_c(\epsilon_s', \gamma, \epsilon_c'), \tag{8}$$

where $F_c(\epsilon_s', \gamma, \epsilon_c')$ is the Klein-Nishina scattering kernel and

$$F_c(\epsilon_s', \gamma, \epsilon_c') = 2q\ln(q) + (1 + 2q)(1 - q) + \frac{1}{2}\frac{(\Gamma_e q)^2}{1 + \Gamma_e q}(1 - q), \tag{9}$$

where $q = \epsilon_c'/\Gamma_e\gamma(1 - \epsilon_c'/\gamma)$, $\Gamma_e = 4\epsilon_s'\gamma$, and $1/4\gamma^2 \leq q \leq 1$ must be satisfied. Therefore, the SSC emission intensity is shown as follows (Chiaberge & Ghisellini 1999):

$$I_c'(\nu_c') = j_c'(\nu_c')R_b. \tag{10}$$

The synchrotron and self-Compton scattering photon's dimensionless energies in the blob frame are written as $\epsilon_{s/c}' = h\nu_{s/c}'/m_e c^2$. The corresponding frequencies in the observer's frame are given by $\nu_{s/c} = \delta_b\nu_{s/c}'/(1 + z)$.

2.2 Inhomogeneous Jet Model

Because of the efficiency of synchrotron self-absorption, a one zone SSC model cannot be used to account for the radio to ultraviolet emission of a TeV blazar, a possibility in explaining this emission is to use the inhomogeneous jet model (Marscher 1980; Konigl 1981; Ghisellini et al. 1985). Thus, we use the model assumed to have a conical jet structure (Ghisellini et al. 1985); the configuration of the emission region is shown by the relation:

$$r = aR, \tag{11}$$

where r is the jet radius, R is the coordinate along the jet, and a is a constant. In such a model, the electron energy distribution is $N(\gamma, R) = K(R)\gamma^{-s}$, where $K(R) = K_0(R_0/R)^n$, $s = 2\alpha_0 + 1$, and α_0 is the spectral index of the radio synchrotron emission; the magnetic field satisfies $B(R) = B_0(R_0/R)^m$ with m being a constant through this relation and some physical parameters are estimated in advance, such as B, B_0, R_0, so we can give the blob position R_x inside the

jet; $\gamma_{\mathrm{cut}}(R) = \gamma_{\mathrm{cut}}(R_0)(R_0/R)^e$ (see details in Ghisellini et al. 1985). The synchrotron emission coefficient and self-absorption coefficient in the jet frame are given:

$$j_{\mathrm{s}}^*(R) = C_1(\alpha_0)K_0 B_0^{1+\alpha_0} \nu_{\mathrm{s}}^{*-\alpha_0}(R_0/R)^{n+m(1+\alpha_0)}, \tag{12}$$

$$k_{\mathrm{s}}^*(R) = D_1(\alpha_0)K_0 B_0^{1.5+\alpha_0} \nu_{\mathrm{s}}^{*-\alpha_0-2.5}(R_0/R)^{n+m(1.5+\alpha_0)}, \tag{13}$$

where $C_1(\alpha_0)$ and $D_1(\alpha_0)$ are given in Blumenthal & Gould (1970) and the whole emission region ranges from R_1 to R_2 at a given frequency ν_{s}^*, where $R_1(\nu_{\mathrm{s}}^*) = R_0(\nu_{\mathrm{m}}^{\mathrm{s}}(R_0)/\nu_{\mathrm{s}}^*)^{1/K_m}$ and $R_2(\nu_{\mathrm{s}}^*) = R_0(\nu_{\mathrm{max}}^{\mathrm{s}}(R_0)/\nu_{\mathrm{s}}^*)^{1/\eta}$ with $K_{\mathrm{m}} = 2[n + m(1.5 + \alpha_0) - 1]/(5 + 2\alpha_0)$ and $\eta = 2e + m$. The physical parameters of this model may be estimated by the observations and other astrophysical properties, such as the mass of the central black hole, etc. (see Katarzyński et al. 2001 in detail).

Using the inhomogeneous jet model (Konigl 1981), Jiang et al. (1998) presented a sample of AGNs that included measurements of the angular size and radio flux density of the VLBI (Very Long Baseline Interferometry) core, and then they found that most of the EGRET sources have similar features compared with the other sources, such as higher Doppler factors δ, smaller viewing angles θ, and so on. Their statistical analysis showed that the Doppler factor δ is correlated with the observed 22 GHz brightness temperature and the relative γ-ray luminosity. Hereafter, this team has done a lot of research work about the radio core in AGNs (e.g., Jiang et al. 2001; Cao & Jiang 2002). Recently, Gu et al. (2009) found a strong correlation between the total luminosity of broad emission lines and the bulk kinetic power of the jets, and also showed a significant correlation between the bulk kinetic power and radio extended luminosity. They then presented evidence that the emission from radio lobes is closely related to the energy flux transported through jets from the central part of AGNs. The observed VLBI core angular size θ_{d} was shown as (Jiang et al. 1998)

$$\theta_{\mathrm{d}} = \frac{r(\tau_{\nu_{\mathrm{s}}=1})\sin\theta}{D_{\mathrm{a}}}, \tag{14}$$

where θ is the angle between the axis of the jet and the direction of the observer, $r(\tau_{\nu_{\mathrm{s}}=1})$ is the distance from the origin of the jet, at which the optical depth to the synchrotron self-absorption at the observing frequency ν_{s} is equal to unity, and D_{a} is the angular diameter distance of the source. With the VLBI measurements of the core angular dimension and radio flux through the relation (Ghisellini et al. 1993)

$$\delta = f(\alpha)F_{\mathrm{m}}\left[\frac{\ln(\nu_{\mathrm{b}}/\nu_{\mathrm{m}})}{F_{\mathrm{x}}\theta_{\mathrm{d}}^{6+4\alpha}\nu_{\mathrm{x}}^{\alpha}\nu_{\mathrm{m}}^{5+3\alpha}}\right]^{1/(4+2\alpha)}(1+z), \tag{15}$$

many physical parameters could be associated with the conical jet. In this case, z and α are, respectively, the red-shift and spectral index, δ is the Doppler factor, F_{m} is the synchrotron flux at the turnover frequency ν_{m}, F_{x} is the X-ray flux at frequency ν_{x}, ν_{b} is the synchrotron cut-off frequency, and the function $f(\alpha) \simeq 0.08\alpha + 0.14$. Here the spectral index of photon energy spectrum α is important to constrain the model parameters in order to deduce precise intrinsic spectra. The observed flux can be enhanced owing to the fact that beaming is δ^p, where $p = 2 + \alpha$ in the case of a continuous conical jet and $p = 3 + \alpha$ in the case of a moving sphere (e.g., Lind & Blandford 1985; Ghisellini et al. 1993; Urry & Padovani 1995).

2.3 Optical Depth

When the emitted photon's frequency is high enough, the Compton photons can interact with the internal synchrotron photons and produce $e^{\pm}$ pairs (Gould & Schréder 1967; Brown et al. 1973; Coppi & Blandford 1990; Inoue & Takahara 1996; Finke et al. 2008). However, this effect does not play an important role in the observed VHE radiation spectrum. Here we only consider the interaction between high energy γ-rays and extragalactic background light (EBL). The absorption

effect of high energy γ-rays has been discussed in many previous papers (e.g., Stecker & De Jager 1998; Malkan & Stecker 1998; Kneiske et al. 2002, 2004; Stecker et al. 2006, 2007; Primack et al. 2005; Dwek & Krennrich 2005; Kneiske & Dole 2008, 2010; Krennrich et al. 2008).

The optical depth depends on the spectral energy distribution of the EBL, and it can be given by the expression (Dwek & Krennrich 2005)

$$\tau_\gamma(E_\gamma, z) = \int_0^z \left(\frac{dl}{dz'}\right)dz' \int_{-1}^{+1} d\mu \frac{1-\mu}{2} \int_{\epsilon'_{\mathrm{th}}}^\infty d\epsilon' n_\epsilon(\epsilon', z')\sigma_{\gamma\gamma}(E'_\gamma, \epsilon', \mu), \qquad (16)$$

where $\sigma_{\gamma\gamma}(E'_\gamma, \epsilon', \mu)$ is the cross section for the $\gamma\gamma$ interaction, and is described as follows (Jauch & Rohrlich 1955):

$$\sigma_{\gamma\gamma}(E'_\gamma, \epsilon', \mu) = \frac{3\sigma_T}{16}(1 - \beta^2) \times \left[2\beta(\beta^2 - 2) + (3 - \beta^4)\ln\left(\frac{1+\beta}{1-\beta}\right)\right] \quad . \qquad (17)$$

where $\beta = \sqrt{1 - \frac{\epsilon_{\mathrm{th}}}{\epsilon}}$, $\epsilon_{\mathrm{th}} = 2(m_e c^2)^2/E_\gamma(1 - \mu)$, $\mu = \cos\theta$ is the angle between the incident photons, and $\sigma_{\mathrm{T}} = 6.65 \times 10^{-25}$ cm^2 is the Thomson cross section.

$$\frac{dl}{dz} = c\frac{dt}{dz} = \frac{R_{\mathrm{H}}}{(1+z)E(z)} \quad , \qquad (18)$$

$$E(z) = \{(1+z)^2(\Omega_m z + 1) + z(2+z)[(1+z)^2\Omega_{\mathrm{r}} - \Omega_\Lambda]\}^{1/2},$$

where the Hubble radius $R_{\mathrm{H}} = c/H_0$, and we adopt a cosmology with the matter density $\Omega_{\mathrm{m}} = 0.3$ and the radiation energy density $\Omega_\Lambda = 0.7$, both normalized to the critical density ($\Omega_{\mathrm{m}} + \Omega_{\mathrm{r}} + \Omega_\Lambda = 1$ in a flat universe); Ω_Λ is the dimensionless cosmological constant. The number density of EBL photons with energy ϵ is shown by Kato et al. (2006)

$$n_\epsilon(\epsilon, z) = \frac{4\pi}{c\epsilon^2}\nu I_\nu(\nu, z) = (1+z)^2 n_0(\nu_0), \qquad (19)$$

where $\nu = \nu'/(1 + z') = \nu_0(1 + z)$, $\epsilon = h\nu$, and $n_0(\nu_0)$ is the EBL number density at $z = 0$.

The twelve different EBL realizations have been generated by Dwek & Krennrich (2005). These EBL templates are expressed as XYZ with X=L, M, H representing the energy fluxes of the stellar components of EBL (L=low, M=medium, or H=high), Y=L or H, and Z=L or H standing for the EBL energy fluxes in the 15 μm band and in the far-IR band respectively. In addition, a strict lower-limit EBL from the ultraviolet to the far-infrared photon energies has been derived by Kneiske & Dole (2008, 2010). It offers a minimum correction for the $\gamma\gamma$ absorption optical depth by the EBL. After considering the absorption effect with EBL, we can reproduce the observed spectrum with the intrinsic spectrum times $e^{-\tau(E_\gamma, z)}$.

3 APPLICATIONS TO H 2356–309 AND 1ES 1218+304

3.1 H 2356–309

H 2356–309 is one of the most distant high frequency peaked BL Lac objects observed with VHE emission, and it shows very strong synchrotron radiation. The X-ray emission of H 2356–309 with a redshift of $z = 0.165$ was first observed by the Small Astronomical Satellite 1 (SAS-1, the UHURU Satellite) launched on 12 December 1970 (Forman et al. 1978). The BeppoSAX Satellite launched on 30 April 1996 has also detected X-ray emission from the H 2356–309 (Costamante et al. 2001). Recently, the data in the VHE γ-ray, the X-ray, and the optical bands were simultaneously observed by the H.E.S.S. Cherenkov telescopes (Aharonian et al. 2006), the RXTE, the NRT and the ROTSE-III in 2004 (Jahoda & PCA Team 1996; Aharonian et al. 2005), respectively. Some observations
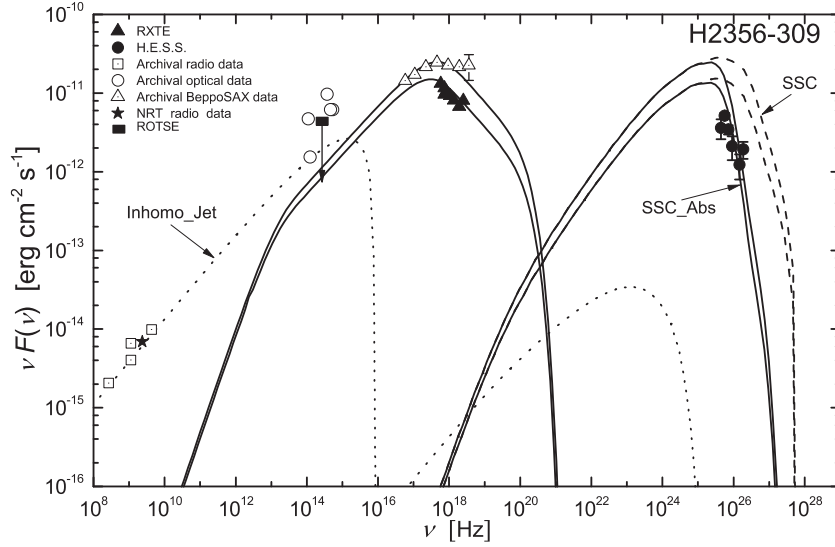
Fig. 1 Comparison of the predicted SEDs with the observed data for the TeV blazar H 2356–309. The dashed lines represent the calculated SEDs in the SSC model without absorptions, dotted lines represent the results in the inhomogeneous model, and solid lines represent resulting values corrected by the strict lower-limit EBL. The physical parameters involved in the calculation are shown in Tables 1 and 2. Data are taken from the Archival, the RXTE, the H.E.S.S. telescopes and the ROTSE (Superina et al. 2006; Costamante et al. 2001; Aharonian et al. 2006; Jahoda & PCA Team 1996; Aharonian et al. 2005). The data from the RXTE, the H.E.S.S. telescopes and the ROTSE are obtained simultaneously.

have revealed that the H 2356–309 is a normal elliptical galaxy (Falomo 1991; Scarpa et al. 2000; Cheung et al. 2003).

In Figure 1, the two multiband spectra corresponding to two (high and low) states of H 2356–309 are shown with different physical parameters given in Tables 1 and 2. These physical parameters of the SSC model may be constrained through some observed quantities, but it is still very difficult to precisely give all parameters, while simultaneously we also have some free choices. It is because the parameters of the inhomogeneous jet model cannot be constrained sufficiently through observations.

Data from the H.E.S.S., the RXTE and the ROTSE-III are well described by the SSC model, in which the magnetic field $B = 0.16$ G and the electron minimum Lorentz factor $\gamma_{\min} = 1000$; other physical parameters are listed in Table 1. With the SSC model, we can find that the energy spectra with two states clearly present the power-law shapes in the X-ray band. At the same time, we consider the absorption by the strict lower-limit EBL (Kneiske & Dole 2008, 2010), thus the very high energy γ-ray spectra are also well reproduced. For the high state, the observations of the VHE γ-ray data are expected with the development of future space-based observing techniques. In the radio band, we fit the SED with the inhomogeneous jet model, in which the best fit for the observed spectral shape is described by the following values: $n = 2$, $m = 0.9$, $e = 0.15$ and $\alpha_0 = 0.45$. Other parameters are given in Table 2; through these physical parameters and some results of the models (as shown in Table 3), we can reproduce the angular size $\theta_{\rm d}$ of the unresolved VLBI core by using Equation (15), thus the $\theta_{\rm d}$ of the H 2356–309 equals 0.05 mas. Under the "blob in jet" scenario, with a crucial parameter B, we can deduce the blob's position $R_{\rm x}$, which is equal to 6.92×10^{17} cm.

Table 1 Physical Parameters Used for SSC Models. The superscripts 'l' and 'h' represent respectively the low and high state of the SEDs for H 2356–309 (see text for details).

Parameter Symbol	H 2356–309$^{\mathrm{l}}$	H 2356–309$^{\mathrm{h}}$	1ES 1218+304
R_{b} (cm)	3.4×10^{15}	3.4×10^{15}	3.0×10^{16}
B (G)	0.16	0.16	0.047
δ_{b}	18.5	19	20
K (cm^{-3})	1.9×10^4	2.3×10^4	2.8×10^2
γ_{brk}	1.62×10^5	2.5×10^5	1.4×10^4
γ_{cut}	3×10^6	3×10^6	1.1×10^6
n_1	2	2	1.8
n_2	4	4	2.9
z	0.165	0.165	0.182

Table 2 Physical Parameters Used for Inhomogeneous Jet Model (see text for details).

Parameter Symbol	H 2356–309	1ES 1218+304
α_0	0.45	0.45
m	0.9	1.2
n	2.0	2.1
e	0.15	0.15
B_0 (G)	0.35	0.2
δ_j	9	10
K_0 (10^2 cm^{-3})	1.0	1.0
$\nu_{\max}(R_0)$ (10^{15} Hz)	1.0	1.0
r_0 (10^{16} cm)	1.0	1.0
R_0 (10^{17} cm)	2.9	2.9
$r_{\max}$ (10^{19} cm)	1.6	1.6
$R_{\max}$ (10^{20} cm)	4.6	4.6
R_{x} (10^{17} cm)	6.92	9.69

Table 3 Physical Parameters Used for Estimating Angular Sizes of Unresolved VLBI Cores

Source	z	θ_{d} (mas)	ν_{X} (keV)	F_{X} (μJy)	ν_{m} (GHz)	F_{m} (Jy)	ν_{b} (10^{15} Hz)
H 2356–309	0.165	0.05	1.0	6.25	5.0	0.18	1.0
1ES 1218+304	0.182	0.02	1.0	5.80	5.0	0.05	1.0

Because of the complex jet properties, to get the exact constraints of the parameters, further analysis is required. Certainly, a high energy synchrotron self-Compton radiation can also be produced, but the effect of this radiation is very small, which can be neglected, as shown in Figure 1.

3.2 1ES 1218+304

At a redshift of $z = 0.182$, the extragalactic source 1ES 1218+304 is also a distant high frequency peaked BL Lac object. The TeV γ-ray emission from it has been detected by the MAGIC (Major Atmospheric Gamma Imaging Cherenkov) telescope (Albert et al. 2006). Recently the VERITAS (Very Energetic Radiation Imaging Telescope Array System) telescope (Fortin 2008) observed the TeV emission of 1ES 1218+304 again and confirmed the outcome of the MAGIC team's findings. The NED database has also given many useful data from the radio up to the X-ray band. The hard X-ray spectrum of 1ES1218+304 was detected with BeppoSAX in July 1999. The EGRET (Energetic Gamma-Ray Experiment Telescope) showed its flux upper limit to be $\sim 10^{-11}$ erg cm^{-2} s^{-1}. In

May 2006, the X-ray astronomy satellite Suzaku detected X-ray emission (Sato et al. 2008), and it presents a clear power-law shape.

In order to reproduce the emission energy spectrum of 1ES 1218+304, we adopt the inhomogeneous model in the jet and the synchrotron self-Compton radiation in the blob. The physical parameters are listed in Tables 1 and 2. The optical contribution from the host galaxy is not included in this paper. The absorption by the strict lower-limit EBL is given to account for the $\gamma\gamma$ absorption optical depth of 1ES 1218+304.
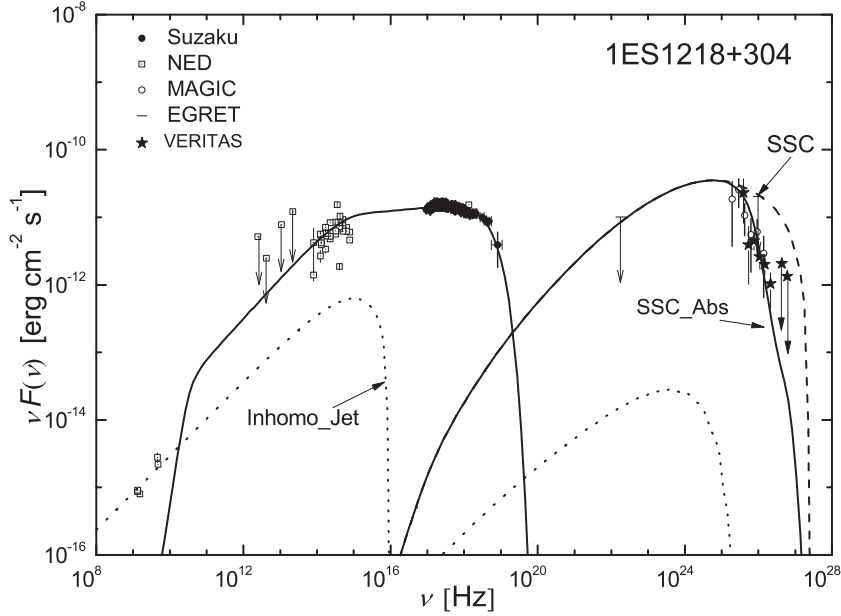
Fig. 2 Comparison of the predicted SEDs with the observed data for the TeV blazar 1ES 1218+304. The dashed line represents the calculated SED in the SSC model without absorption, dotted lines represent the results in the inhomogeneous model, and solid lines represent resulting values corrected by the strict lower-limit EBL. The physical parameters involved in the calculation are shown in Tables 1 and 2. Data are obtained by the Suzaku, the MAGIC, the VERITAS, and the NED database, and the upper limits are given by the EGRET (Sato et al. 2008; Albert et al. 2006; Fortin & Pascal 2008).

In Figure 2, the data from Suzaku distinctly show a power-law shape with a cut-off, and we explain the observed X-ray power-law spectrum well with the one-zone homogeneous SSC model, in which the canonical index $n_1 = 1.8$ is shown for the low energy end and $n_2 = 2.9$ for the high energy end. With the characteristic variability time scale of the flare $t \simeq 5 \times 10^4$ s, we give $R_b = ct\delta_b/(1+z) \simeq 3 \times 10^{16}$ cm with the moderate Doppler factor $\delta_b = 20$. In the SSC model, data from the NED database can also be well explained with $\gamma_{min} = 1$, $\gamma_{brk} = 1.4 \times 10^4$ and $\gamma_{cut} = 1.1 \times 10^6$. The high energy γ-ray data from MAGIC and VERITAS can be fitted with the $\gamma\gamma$ absorption by the strict lower-limit EBL. The other parameters of the one-zone homogeneous SSC model are listed in Table 1. In view of the data for the radio band, similarly, we fitted the spectra with the inhomogeneous jet model, in which the spectral shape is depicted by the parameters $n = 2.1$, $m = 1.2$, $e = 0.15$, and $\alpha_0 = 0.45$ With these parameters and our results of the models (see Table 3

in detail), we also find that θ_d of the 1ES 1218+304 is equal to 0.02 mas. Similarly, we give the location of the blob with R_x equaling 9.69×10^{17} cm. Here the weak effect from the jet synchrotron self-Compton scattering is also neglected, as shown in Figure 1, and the contribution from the host galaxy is also not analyzed in this paper.

4 SUMMARY AND DISCUSSION

In this paper, the spectral energy distributions (SEDs) of two TeV blazars H 2356–309 and 1ES 1218+304 can be well reproduced with the inhomogeneous jet model and the homogeneous SSC model, which indicates that the leptonic models are very successful in explaining multi-band emissions of TeV blazars. Obviously, the emissions of the X-ray bands are from the synchrotron radiation of the relativistic electrons, and the VHE γ-rays are produced by the synchrotron self-Compton scattering in a one-zone homogeneous blob; the corresponding SSC emission from the conical jet is negligible. For these two sources, we could reproduce the angular sizes of the unresolved VLBI cores by the above theoretical models. The accurate values are left out from further development of the VLBI survey. Here we do not consider the EIC model due to its weak influence on the non-thermal spectra of HBLs. However, the EIC effect must be further considered for FSRQs and LBLs (Böttcher 2007). With data of the H 2356–309 from the BeppoSAX satellite, we can predict the existence of the TeV γ-ray emission to be consistent with the high state of H 2356–309. The absorption by $\gamma\gamma$ interactions are calculated with a strict lower-limit EBL. Namely, a minimum correction is constructed to depict the observed SED of a TeV blazar.

With the development of the space telescope technique, like the recently launched Fermi Gamma-ray Space Telescope (FGST), we will find more information and further understand the emission mechanisms of particle acceleration in blazars. We expect more new data from the observations of AGNs by the FGST, Suzaku, and so on, in the next few years. Because of the uncertain EBL, we may further reproduce the EBL spectrum and analyze the light curve of the TeV blazar in future work.

References

Aharonian, F. A. 2000, New Astron., 5, 377
Aharonian, F. A., et al. 2005, A&A, 442, 895
Aharonian, F. A., et al. 2006, A&A, 449, 223
Albert, J., et al. 2006, ApJ, 642, L119
Atoyan, A., & Dermer, C. D. 2003, ApJ, 586, 79
Błażejowski, M., et al. 2000, ApJ, 545, 107
Bloom, S. D., & Marscher, A. P. 1996, ApJ, 461, 657
Blumenthal, G. R., & Gould, R. J. 1970, Rev. of Modern Phys., 42, 237
Böttcher, M., & Reimer, A. 2004, ApJ, 609, 576
Böttcher, M. 2007, Ap&SS, 309, 95
Brown, R. W., Mikaelian, K. O., & Gould, R. J. 1973, Astrophys. Lett., 14, 203
Cao, X. W., & Jiang, D. R. 2002, MNRAS, 331, 111
Cheung, C. C., Urry, C. M., Scarpa, R., & Giavalisco, M. 2003, ApJ, 599, 155
Chiaberge, M., & Ghisellini, G. 1999, MNRAS, 306, 551
Coppi, P. S., & Blandford, R. D. 1990, MNRAS, 245, 453
Costamante, L., Ghisellini, G., Giommi, P., et al. 2001, A&A, 371, 512

Crusius, A., & Schlickeiser, R. 1986, A&A, 164, L16

Dermer, C. D., Sturner, S. J., & Schlickeiser, R. 1997, ApJS, 109, 103

Dermer, C. D. 1999, Astropart. Phys., 11, 1

Dwek, E., & Krennrich, F. 2005, ApJ, 618, 657

Falomo, R. 1991, AJ, 101, 821

Finke, J. D., Dermer, C. D., & Böttcher, M. 2008, ApJ, 686, 181

Forman, W., Jones, C., Cominsky, L., et al. 1978, ApJS, 38, 357

Fortin, P. 2008, American Institute of Physics Conference Series, 1085, 565 (arXiv:0810.0301)

Ghisellini, G., Maraschi, L., & Treves, A. 1985, A&A, 146, 204

Ghisellini, G., Guilbert, P., & Svensson, R. 1988, ApJ, 334, L5

Ghisellini, G., Padovani, P., Celotti, A., & Maraschi, L. 1993, ApJ, 407, 65

Ghisellini, G., & Madau, P. 1996, MNRAS, 280, 67

Giommi, P., & Padovani, P. 1994, MNRAS, 268, L51

Gould, R. J., & Schréder, G. P. 1967, Phys. Rev., 155, 1404

Gu, M. F., Cao, X. W., & Jiang, D. R. 2009, MNRAS, 396, 984

Hartman, R. C., et al. 2001, ApJ, 553, 683

Inoue, S., & Takahara, F. 1996, ApJ, 463, 555

Jahoda, K., et al. 1996, Bulletin of the American Astronomical Society, 28, 1285

Jauch, J. M., & Rohrlich, F. 1955, The Theory of Photons and Electrons (Cambridge: Addison-Wesley)

Jiang, D. R., Cao, X. W., & Hong, X. Y. 1998, ApJ, 494, 139

Jiang, D. R., Cao, X. W., & Zhou, J. F. 2001, IAUS, 205, 148

Jones, F. C. 1968, Phys. Rev., 167, 1159

Kardashev, N. S. 1962, Soviet Astron., 6, 317

Kataoka, J., Mattox, J. R., Quinn, J., et al. 1999, ApJ, 514, 138

Katarzyński, K., Sol, H., & Kus, A. 2001, A&A, 367, 809

Katarzyński, K., Sol, H., & Kus, A. 2003, A&A, 410, 101

Kato, T., Kusunose, M., & Takahara, F. 2006, ApJ, 638, 653

Kirk, J. G., Rieger, F. M., & Mastichiadis, A. 1998, A&A, 333, 452

Kneiske, T. M., Mannheim, K., & Hartmann, D. 2002, A&A, 386, 1

Kneiske, T. M., Bretz, T., Mannheim, K., & Hartmann, D. 2004, A&A, 413, 807

Kneiske, T. M., & Dole, H. 2008, AIPC, 1085, 620

Kneiske, T. M., & Dole, H. 2010, arXiv:1001.2132

Konigl, A. 1981, ApJ, 243, 700

Krawczynski, H., Coppi, P. S., & Aharonian, F. 2002, MNRAS, 336, 721

Krennrich, F., Dwek, E., & Imran, A. 2008, ApJ, 689, L93

Kusunose, M., & Takahara, F. 2005, ApJ, 621,285

Lind, K. R., & Blandford, R. D. 1985, ApJ, 295, 358

Malkan, M. A., & Stecker, F. W. 1998, ApJ, 496, 13

Mannheim, K., & Biermann, P. L. 1992, A&A, 253, L21

Mannheim, K. 1993, A&A, 269, 67

Maraschi, L., Ghisellini, G., & Celotti, A. 1992, ApJ, 397, L5

Marscher, A. P. 1980, ApJ, 235, 386

Marscher, A. P., & Gear, W. K. 1985, ApJ, 298, 114

Mücke, A., & Protheroe, R. J. 2000, AIPC, 515., 149

Mücke, A., et al. 2003, Astropart. Phys., 18, 593

O'dell, S. L. 1988, ApJ, 327, 60

Pohl, M., & Schlickeiser, R. 2000, A&A, 354, 395

Primack, J. R., Bullock, J. S., & Somerville, R. S. 2005, High Energy Gamma-Ray Astronomy, 745, 23

Rachen, J., & Mészáros, P. 1998, Phys. Rev. D, 58, 123005

Rybicki, G., & Lightman, A. P. 1979, Radiative Processes in Astrophysics (New York: Wiley Interscience)

Sambruna, R., et al. 1997, ApJ, 474, 639

Sato, R., Kataoka, J., et al. 2008, ApJ, 680, L9

Scarpa, R., Urry, C. M., Padovani, P., Calzetti, D., & O'Dowd, M. 2000, ApJ, 544, 258

Sikora, M., Begelman, M. C., & Rees, M. J. 1994, ApJ, 421, 153

Stecker, F. W., & De Jager, O. C. 1998, A&A, 334, L85

Stecker, F. W., Malkan, M. A., & Scully, S. T. 2006, ApJ, 648, 774

Stecker, F. W., Malkan, M. A., & Scully, S. T. 2007, ApJ, 658, 1392

Superina, G., & The H. E. S. S Collaboration 2006, SF2A-2006: Proceedings of the Annual meeting of the French Society of Astronomy and Astrophysics, eds. D. Barret, F. Casoli, G. Lagache, A. Lecavelier, & L. Pagani, 193

Tavecchio, F., Maraschi, L., & Ghisellini, G. 1998, ApJ, 509, 608 (TMG)

Urry, C. M., & Padovani, P. 1995, PASP, 107, 803